The peculiar cluster HS 327 in the Large Magellanic Cloud: Can OH/IR stars and carbon stars be twins?

J. Th. van Loon, A. A. Zijlstra, L. Kaper, G. F. Gilmore, C. Loup, J. A. D. L. Blommaert

A&A 368, 239–249 (2001)
DOI: 10.1051/0004-6361:20000529

Astronomy & Astrophysics

The peculiar cluster HS 327 in the Large Magellanic Cloud: Can OH/IR stars and carbon stars be twins?⋆

J. Th. van Loon[1], A. A. Zijlstra[2], L. Kaper[3], G. F. Gilmore[1], C. Loup[4], and J. A. D. L. Blommaert[5]

[1] Institute of Astronomy, Madingley Road, Cambridge CB3 0HA, UK
[2] UMIST, PO Box 88, Manchester M60 1QD, UK
[3] Astronomical Institute, University of Amsterdam, Kruislaan 403, 1098 SJ Amsterdam, The Netherlands
[4] Institut d'Astrophysique de Paris, 98bis Boulevard Arago, 75014 Paris, France
[5] ISO Data Centre, Astrophysics Div., Science Dept. of ESA, Villafranca del Castillo, PO Box 50727, 28080 Madrid, Spain

Received 29 September 2000 / Accepted 19 December 2000

Abstract. The obscured OH/IR star IRAS 05298−6957 in the LMC was recently noticed to be member of the small double cluster HS 327 that also contains a carbon star (van Loon, et al. 1998, A&A, 329, 169). Hence they are coeval and have (nearly) the same progenitor mass, which can only be understood if Hot Bottom Burning (HBB) has prevented IRAS 05298−6957 from being a carbon star. We present extensive visual and near-IR photometric data for $>10^4$ stars in and around HS 327, and spectroscopic data for some of the brightest AGB stars amongst these. Colour-magnitude diagrams are used to estimate the age for the cluster and its members, and luminosities are derived for the stars for which spectra have been obtained. The age for IRAS 05298−6957 and the carbon star is estimated to be ∼200 Myr. This corresponds to a Main-Sequence progenitor mass ∼4.0 $M_\odot$ – the first direct measurement of the lower mass threshold for HBB. This agrees with stellar evolution models that, however, fail to reproduce the low luminosity of the carbon star.

Key words. stars: carbon – stars: evolution – stars: AGB and post-AGB – open clusters and associations: general – Magellanic Clouds – infrared: stars

1. Introduction

Stars of intermediate mass (∼1 to 8 $M_\odot$) evolve along the Asymptotic Giant Branch (AGB) before ending their life as a white dwarf (Iben & Renzini 1983). The energy production during the final part of the AGB ascent normally takes place in a hydrogen shell surrounding the degenerated carbon-oxygen core, but episodically an inner helium shell ignites (thermal pulse = TP) which may cause material enriched with the products of nuclear processing such as carbon and s-process elements to enter the convective mantle. This is called 3rd dredge-up, and may result in a photospheric C/O ratio exceeding unity, creating a carbon star. Thus the most luminous AGB stars are expected to be carbon stars. These concepts seem to be confirmed by the observation that in clusters in the Large Magellanic Cloud (LMC) no M-type stars are found brighter than the brightest carbon star in that cluster (Aaronson & Mould 1985; Westerlund et al. 1991).

The relative efficiency of the 3rd dredge-up is higher for lower metallicity, leading to the prediction of a large population of carbon stars in the Magellanic Clouds (Iben 1981). Hence, the lack of observed carbon stars with luminosities greater than $M_{\rm bol} = -6$ mag, a full magnitude below the AGB-tip luminosity, came as a surprise (Iben 1981; Costa & Frogel 1996). Several reasons for this have been suggested, of which the most promising are that carbon star formation is avoided by nuclear processing of carbon into oxygen and nitrogen at the base of the convective mantle for the most massive AGB stars (Hot Bottom Burning = HBB: Iben & Renzini 1983; Wood et al. 1983), or that luminous carbon stars become invisible at wavelengths shortward of ∼1 μm due to obscuration by a circumstellar dust shell as a result of intense mass loss on the TP-AGB. Recent theoretical work confirms the occurrence of HBB in massive AGB stars with LMC metallicity (Boothroyd et al. 1993; Frost et al. 1998; Marigo et al. 1998), and luminous obscured carbon stars have recently been found in the LMC (van Loon et al. 1997, 1998, 1999a,b; Trams et al. 1999a).

Send offprint requests to: J. Th. van Loon,
e-mail: jacco@ast.cam.ac.uk

⋆ Based on observations obtained at the European Southern Observatory (La Silla, Chile).

The luminous OH/IR star IRAS 05298−6957 (Wood et al. 1992) was noticed by van Loon et al. (1998) to be situated in the core of the small cluster HS 327, and hence it may be possible to estimate its age by comparison of the Colour-Magnitude Diagram (CMD) with theoretical isochrones. They also serendipitously discovered a carbon star in the same cluster. This observation suggests that carbon stars and (oxygen-rich) OH/IR stars may be coeval. More TP-AGB stars have recently been identified in LMC clusters by Tanabé et al. (1997).

We have obtained optical and near-IR imaging photometry for the HS 327 cluster and surroundings, and (limited) spectroscopic observations for some of the brighter stars, in order to derive an age for the stars in the HS 327 cluster. The results are presented, and the implications for AGB evolution and carbon star formation are discussed.

2. Observations

2.1. Gunn gri-band imaging with the Dutch 0.9 m

The direct imaging camera at the Dutch 0.9 m telescope at La Silla, Chile, was used on the six nights of December 25 to 30, 1996, to obtain deep images of a $3.77' \times 3.77'$ region around the cluster HS 327, through Gunn g ($\lambda_0 = 5148$ Å, $\Delta\lambda = 81$ Å), r ($\lambda_0 = 6696$ Å, $\Delta\lambda = 103$ Å) and i ($\lambda_0 = 7972$ Å, $\Delta\lambda = 141$ Å) filters (Thuan & Gunn 1976; Wade et al. 1979). The total integration time amounts to $3^{\rm h}45^{\rm m}$ per filter, split into 5 min exposures to avoid saturation and to allow for refocussing in order to reach the best image quality. The pixels measure $0.442'' \times 0.442''$ on the sky, and stellar images on the combined (shift-added) frames have a $FWHM$ of $\sim$1.5″, though some individual frames show stellar images of $\lesssim$1.1″ $FWHM$. The CCD frames were reduced using standard procedures within the ESO-MIDAS package. The photometry was calibrated by means of regular observations of standard stars (see Appendix A and Sect. 3.3 for more details).

2.2. K_s-band imaging with SOFI at the ESO/NTT

SOFI at the ESO 3.5 m NTT at La Silla, Chile, was used on February 15, 1999, to obtain a $K_{\rm s}$-band ($\lambda_0 = 2.162$ μm, $\Delta\lambda = 0.275$ μm) image of HS 327 in order to identify the counterpart of IRAS 05298−6957 and to derive accurate bolometric luminosities for the brightest stars in the vicinity of HS 327. Nine dithered images, each of 10×2 s integration time were combined into one image with an effective integration time of 3 min, at an airmass of 1.322. Standard near-IR observing and data reduction techniques were employed. The sky background was derived from the median of the individual frames, and subtracted. The pixels measure $0.292'' \times 0.292''$ on the sky, and stellar images on the final frame have a $FWHM$ of $\sim$1.0″. For photometric calibration the NICMOS standard star S 121-E ($K_{\rm s} = 11.781 \pm 0.005$ mag) was observed at an airmass of 1.224 by combining five shifted images, each of 10×2 s integration time.

2.3. I-band spectroscopy with EMMI at the ESO/NTT

EMMI at the ESO 3.5 m NTT at La Silla, Chile, was used on February 4, 1996, to obtain low-resolution ($R \sim 500$; grism #4) spectra between $\sim$0.61 and 1.0 μm. The goal was to obtain a spectrum of IRAS 05298−6957, but this was unsuccessful. However, four stars in the vicinity of IRAS 05298−6957 were identified from their red colours on V and I-band acquisition images: $(V-I) \sim 3$ to 4 mag, compared to normal red giants that have $(V-I) \sim 1$ to 2 mag. One of these is a carbon star, which spectrum was published and discussed in van Loon et al. (1998). Here the results for the other three stars are presented. All spectra were exposed for 5 min. The CCD frames were corrected for the electronic offset (bias) and for the relative pixel response (flatfield). Wavelength calibration was performed relative to He+Ar lamp spectra. The sky-subtracted spectra were then corrected for the wavelength dependence of the instrumental response as measured from a spectrum of the standard star LTT 1020, and for atmospheric continuum extinction.

2.4. I-band spectroscopy with EFOSC II at the ESO/3.6 m

EFOSC II at the ESO 3.6 m telescope at La Silla, Chile, was used on July 5, 2000, to obtain a low-resolution ($R \sim 400$; grism #12) spectrum between 0.60 and 1.03 μm of a very red point source that was discovered on the $K_{\rm s}$-band image, near HS 327. The spectrum was exposed 25 min. Data reduction was analogous to the EMMI spectra, but the observed standard star was LTT 7379. An appropriate filter was applied to remove charges from the impact of energetic particles. Flexure was found to be negligible. The thin, back-illuminated CCD #40 in use with EFOSC II causes severe fringing at wavelengths $\lambda \gtrsim 0.8$ μm. The telluric emission lines of the sky at dawn were especially bright and difficult to remove: preference was given to an accurate stellar continuum determination for $\lambda \lesssim 0.7$ μm, which in the crowded field allowed only small patches of sky near the object to be taken.

3. Analysis

3.1. Cluster morphology

The open cluster HS 327 (Hodge & Sexton 1966) is poor but rather compact, measuring $\sim$0.5′ across ($\sim$7 pc at the 50 kpc distance to the LMC). Close inspection of the region revealed an accompanying loose cluster of stars, that we call HS 327-E (East), at a distance of $\sim$45″ from the western cluster HS 327-W originally listed by Hodge & Sexton (Figs. 1 and 2). The HS 327-E component may be identified with the small faint cluster KMK 59 (Kontizas er al. 1988), but there is some confusion: SIMBAD's (J2000.0) $\alpha = 5^{\rm h}29^{\rm m}23^{\rm s}\delta = -69°55'18''$ would indeed identify KMK 59 with HS 327-E, but Kontizas et al. themselves give (converted to J2000.0)

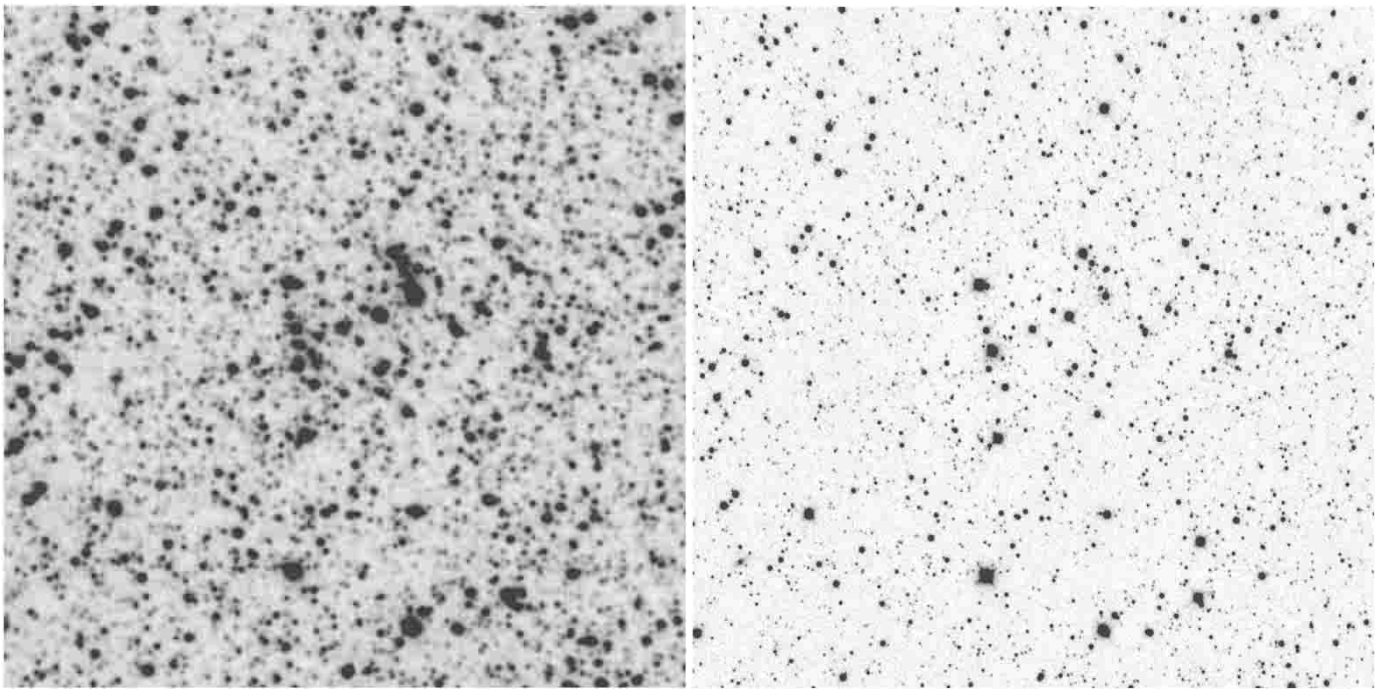

Fig. 1. Dutch 0.9 m Gunn-i (left) and NTT/SOFI $K_{\rm s}$-band (right) images of the region around the LMC cluster HS 327. North is up and East to the left; the edge measures $3'40''$ on the sky

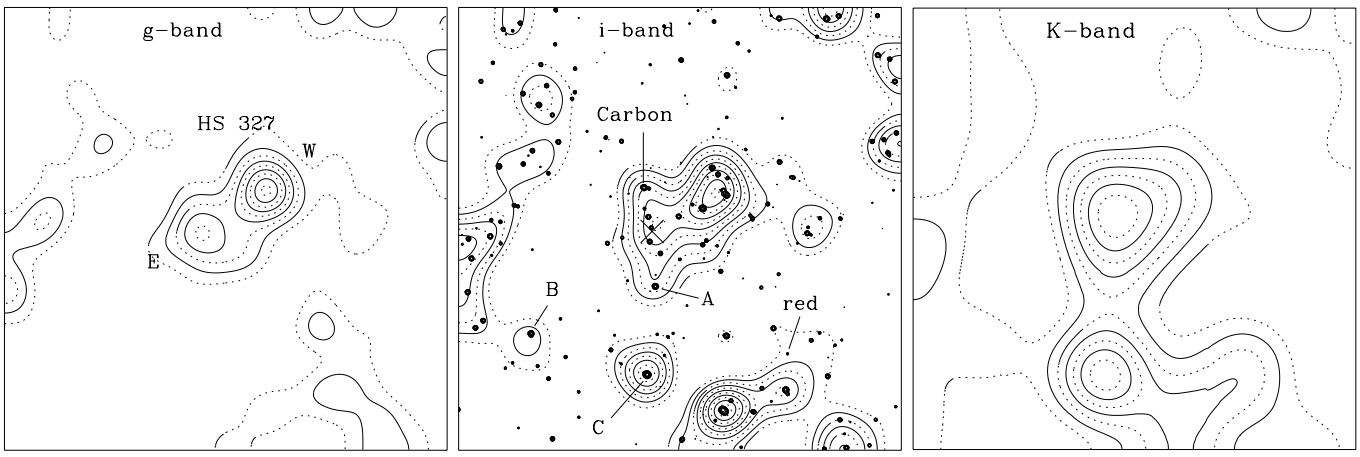

Fig. 2. Brightness contours in Gunn g (left), i (middle) and $K_{\rm s}$ (right). The i-band map is overlaid with the brightest stars, of which the carbon star and the other three stars of which spectra were taken are labelled, as well as the serendipitously discovered red star. The cross indicates the position of IRAS 05298−6957. Orientation and field size are the same as in Fig. 1

$\alpha = 5^{\rm h}28^{\rm m}56^{\rm s}\delta = -69°55'28''$, placing KMK 59 $\sim 2.5'$ to the West of HS 327-E. The Second Generation Digitized Sky Survey does not show anything obvious at Kontizas et al.'s position.

The morphology of the cluster pair becomes apparent when brightness contours are constructed from the images after smoothing by a Gaussian filter with $\sigma = 17.5''$ (Fig. 2). HS 327 stands out most conspicuously in the g-band because bright blue field stars are relatively rare. The visible star density is highest in the i-band, where several individual bright (red) stars add detailed structure to the morphology of the cluster as well as some peaks not associated with the cluster. In the $K_{\rm s}$-band bright stars become rare again, and only one of these (star "C") causes a peak rivalling the cluster contours. What is most intriguing is that HS 327-W is blue, whilst HS 327-E is red.

The brightest stars are overlaid on the i-band image (Fig. 2) to aid in comparing the overall morphology with the location of individual sources. The stars for which spectra have been obtained are labelled: the carbon star ("carbon": van Loon et al. 1998), three M-type stars ("A", "B" and "C"), and a very red carbon star ("red") discovered on the $K_{\rm s}$-band image, as well as the location of the OH/IR star IRAS 05298−6957 (cross).

The near-IR counterpart of IRAS 05298−6957 is very prominent in the $K_{\rm s}$-band image, but (completely) invisible in the i-band image (Fig. 3). Notice the blue star very near IRAS 05298−6957. The 30 s i-band acquisition image

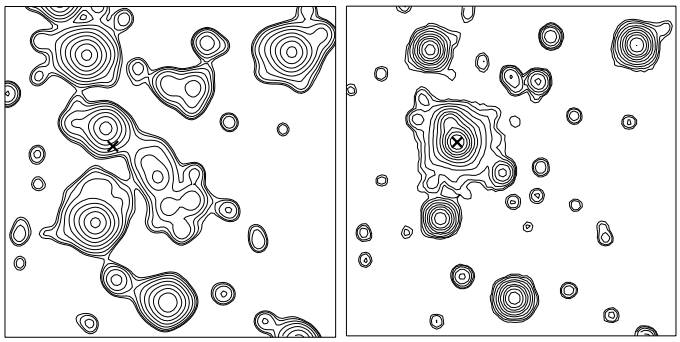

Fig. 3. Dutch 0.9 m Gunn-i (left) and NTT/SOFI K_s-band (right) images of the immediate surroundings of IRAS 05298−6957. North is up and East to the left; the edge measures 24″ on the sky. The cross marks the position of the near-IR counterpart of IRAS 05298−6957

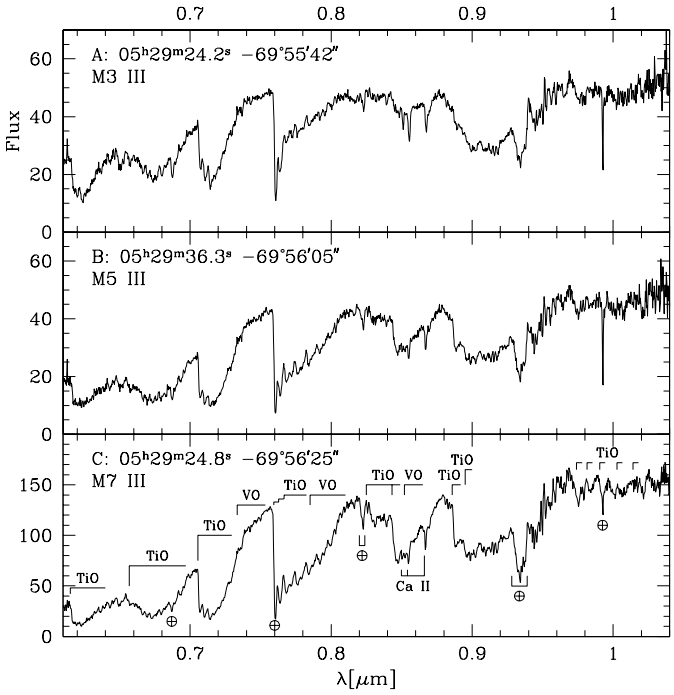

Fig. 4. NTT/EMMI spectra of M-type stars near HS 327

obtained with EFOSC II for the spectroscopy of the very red star in the same field reached the same depth thanks to the greater collecting area of the ESO/3.6 m telescope and the ∼1″ stellar images.

3.2. Cluster membership

IRAS 05298−6957, the carbon star and possibly also star "A" are seen in projection against the Eastern part of the HS 327 cluster complex. How likely is their physical association with the HS 327-E cluster?

Besides IRAS 05298−6957 itself, there are five similarly bright mid-IR point sources within a radius of 10′ from HS 327-E, and these are probably not all obscured AGB stars. This corresponds to a surface density of <70 obscured AGB stars per square degree, or a $\lesssim$6% chance coincidence of an obscured AGB star within 1′ of HS 327-E.

Similarly, there are nine known carbon stars including the cluster member, and one additional possible carbon star, within a radius of 10′ from HS 327-E. This corresponds to a surface density of ∼100 carbon stars per square degree, or a 10% chance coincidence of a field carbon star within 1′ of HS 327-E. The nearest known carbon star other than the cluster member or the very red carbon star is SHV 0530080−695949 at 2.7′.

Star "A" is a moderately luminous M-type star, which are less rare objects than OH/IR stars or carbon stars. Indeed, the two similar stars "B" and "C" are found within 2′ from HS 327. With three such objects in a field >10× the projected size of the cluster complex, the chance of encountering star "A" within the cluster boundaries by coincidence is $\lesssim$30%.

Thus it is highly likely that both the OH/IR star IRAS 05298−6957 and the cluster carbon star are physical members of HS 327-E, and probably the M-type AGB star "A" too. The M-type stars "B" and "C" and the very red carbon star ("red") are considered not to belong to the cluster complex, as they are all situated well outside the faintest brightness contour that isolates the double cluster from the surrounding field.

3.3. Spectral types

Spectra are now available for the brightest and reddest IR point sources in the field around HS 327, which can be used to confirm that these are AGB stars and to determine whether they are oxygen-rich (M-type) or carbon stars.

The spectra of stars "A", "B" and "C" are presented in Fig. 4 in arbitrary flux units, together with their J2000.0 coordinates. The spectra are classified by comparison with Turnshek et al. (1985). They are all M-type: strong TiO absorption bands dominate, and absorption by VO becomes noticable for the cooler star "C". The Ca II triplet is clearly visible in all three stars, and reflects slight redshifts consistent with these stars being members of the LMC. The Ca II strength and the estimated luminosities (Sect. 3.8 and Table 2) indicate they are AGB stars.

The OH/IR star IRAS 05298−6957 was already known to be an oxygen-rich AGB star: spectra in the 3 to 14 μm region indicate the presence of oxygen-rich circumstellar dust (van Loon et al. 1999a; Trams et al. 1999b), and a 1.6 GHz spectrum of OH maser emission suggests LMC membership and a wind velocity of ∼11 km s^{-1}.

The spectrum for the "red" star is presented in Fig. 5 in arbitrary flux units, together with the J2000.0 coordinates. The reddened continuum shows weak absorption of the strongest CN series and of C_2 near 0.77 μm, identifying this star unambiguously as a carbon star. The star may be only moderately carbon-rich and/or rather warm. The absence of the Ca II triplet around 0.86 μm might indicate that the photosphere is of low metallicity altogether.

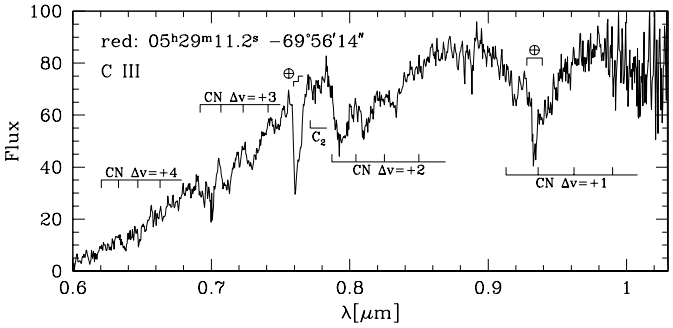

Fig. 5. ESO 3.6 m/EFOSC II spectrum of the very red carbon star near HS 327

It is difficult to assign a spectral sub-type, but the overall appearance and the lack of any conspicuous features that prove otherwise suggest that it is of N-type, i.e. carbon enriched by 3$^{\rm rd}$ dredge-up on the TP-AGB. (cf. Turnshek et al. 1985; Barnbaum et al. 1996).

For the spectrum of the cluster carbon star the reader is referred to van Loon et al. (1998). They argue that it is an AGB star, which agrees with the estimated luminosity (Sect. 3.8 and Table 2).

3.4. Multi-object photometry

Multi-object photometry was performed on the images using an implementation of DAOPHOT (version II) and ALLSTAR (Stetson 1987) within ESO-MIDAS.

The Point Spread Function (PSF) was represented by an analytic Moffat function with $\beta = 2.5$ plus a quadratic lookup table to take into account variations in the shape of the PSF across the frame. This PSF was established using bright, relatively isolated stars in an iterative scheme involving subtraction of contaminating neighbour stars. The multi-object photometry itself comprised between several and a dozen passes (per filter) through DAOPHOT & ALLSTAR, each time subtracting already measured stars in order to also find and measure fainter and/or blended stars. This resulted in the detection of $\sim$2.4 10^4 sources in each of the gri-bands, and $\sim$1.0 10^4 stars in the K-band in the 3.7 10^{-3} square degree area around HS 327.

The photometric calibration was established by comparison of aperture photometry on the standard star images with aperture photometry on a (few) dozen bright stars in the images of the HS 327 area (after subtracting contaminating neighbour stars using PSF fitting). The multiple-object PSF photometry was then scaled accordingly. The calibration of the gri-band photometry, correcting for airmass dependencies of the photometric zero point, is mainly based on the December 25 night but the photometric zero point has been checked for the other nights too (see also Appendix A). Photometric calibration errors are unlikely to exceed a few %.

The completeness and photometric errors were estimated by a restricted number of artificial star experiments. Incompleteness is mainly due to blending and/or positional discrepancies as a result of crowding. The i-band point-source extraction reaches a completeness level of 98% at $i \sim 18.75$ mag, dropping to 55% and 5% at $i \sim 21.75$ and 23.75 mag, respectively. For stars with $i \gtrsim 22.25$ mag the error on the photometry is $\gtrsim$1 mag, with magnitudes systematically too bright by $\gtrsim$0.1 mag. The g and r-bands go $\sim$0.75 mag deeper. The K-band images reach $K_{\rm s} \sim 19$ mag.

Point-sources were cross-correlated between the different filters after geometric transformation (rotation and linear translation), using an iterative scheme with a growing search radius, and rejecting extended sources on the basis of the sharpness parameter returned by ALLSTAR.

3.5. Colour-magnitude diagrams

The i versus $(g-i)$ and $K_{\rm s}$ versus $(i-K_{\rm s})$ CMDs are given in Fig. 6 for the HS 327 cluster and surrounding field. The cluster boundaries were defined by a rectangular box encompassing the faintest solid i-band contour in Fig. 2. The red stars for which spectra have been obtained are labelled, and the location of the AGB, RGB and Main Sequence are indicated. The $K_{\rm s}$-band image barely reaches as faint as the Main Sequence. The reddening vector is determined by convolving the extinction curve compiled by Mathis (1990) with a Vega model (Kurucz 1993), yielding extinction coefficients $A_\lambda/A_V = 1.094$, 0.796, 0.621 and 0.112 for the gri- and $K_{\rm s}$-bands, respectively. Stars of other spectral types have somewhat different extinction coefficients, especially at shorter wavelengths. Kurucz (1993) and Fluks et al. (1994) spectra are used to transform the isochrones of Bertelli et al. (1994) into CMDs, taking into account the filter and CCD response curves. The metallicity of the intermediate-age population is assumed to be [metals/H] $= -0.4$ (typical for the LMC).

The field contains stars with ages ranging from $\sim$0.1 to $\sim$10 Gyr. The age of the oldest stars is not very accurate because isochrones for stars of such ages do not differ much in colours and the photometry becomes incomplete above the Main Sequence turn-off for stars older than a few Gyr. Also, the reddening of the stars with respect to the isochrones is a priori unknown, although the general look of the CMDs suggests a visual extinction of no more than a few 0.1 mag.

3.6. Colour-colour diagrams

Colour-colour diagrams have the potential to identify stars with particular spectral signatures, such as carbon stars. In oxygen-rich cool stars the g-, r- and i-bands include TiO absorption, with the i-band also including VO absorption that is present in the coolest stars. In carbon stars the g-band includes C_2 absorption, and the r- and i-bands include CN absorption (stronger in the i-band). The $K_{\rm s}$-band mainly measures the continuum.

The carbon stars indeed exhibit somewhat different colours from the M-type stars (Fig. 7). Carbon stars may have bluer $(g-i)$ colours than M-type stars if they do

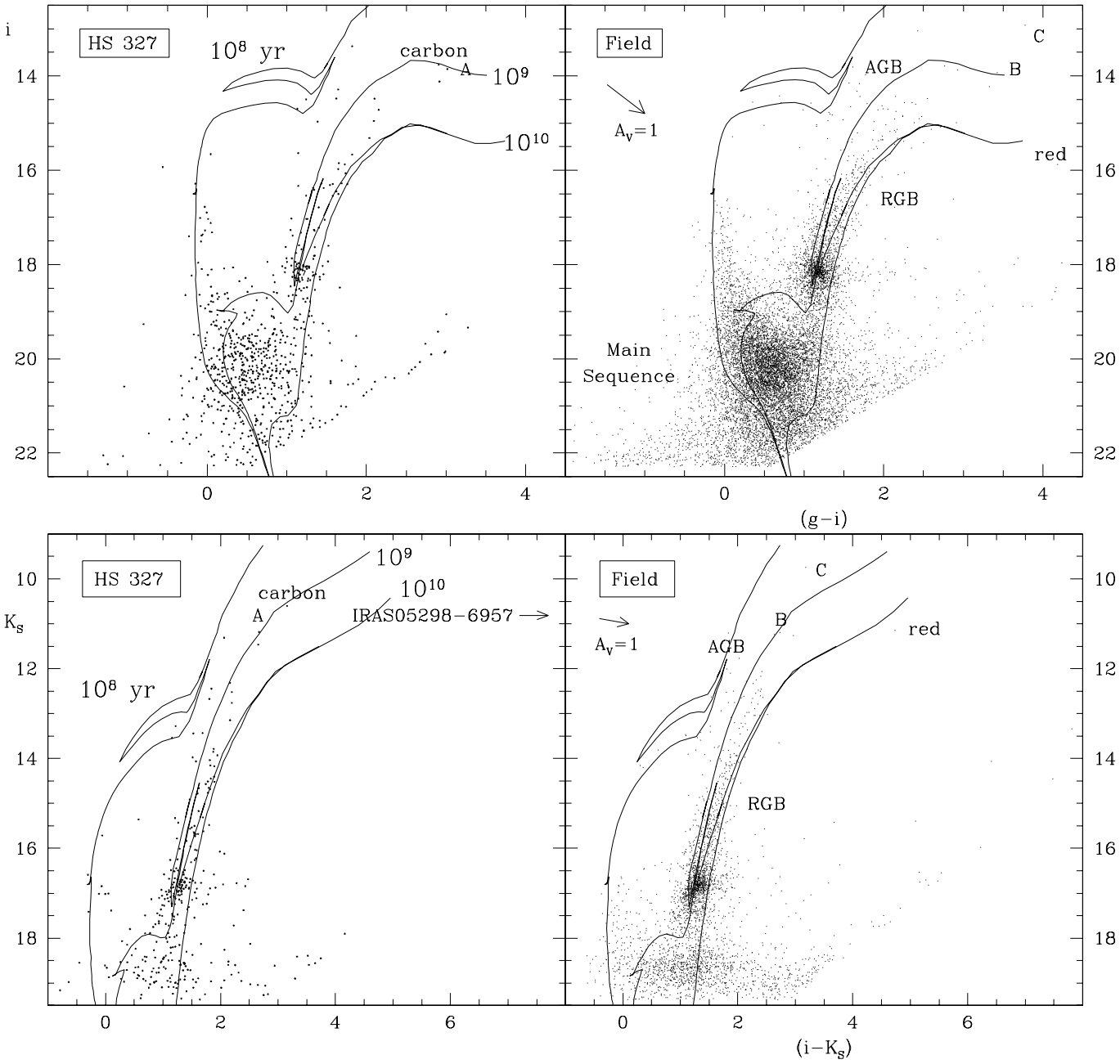

Fig. 6. CMDs of i versus $(g-i)$ (top) and K_s versus $(i-K_\mathrm{s})$ (bottom) for the double cluster HS 327 (left) and surrounding field (right). Stars whose spectra have been taken are labelled, and the location of the AGB, RGB and Main Sequence are indicated. Isochrones (Bertelli et al. 1994) are plotted for [metals/H] $= -0.4$, and ages of 10^8, 10^9 and 10^{10} yr

not have very strong C_2 bands that absorb in the g-band, because the g-band intensity of M-type stars is suppressed by TiO absorption. As can clearly be seen in the synthetic, solar-metallicity M-type spectra from Fluks et al. (1994), the coolest M-type stars have relatively red $(i-K_\mathrm{s})$ for their $(g-i)$ colours due to the TiO and VO absorption that affects the i-band. The same happens for the carbon stars, but now it is due to the CN absorption in the i-band.

There is only a small mismatch between the synthetic colours for M 0 to M 3 stars and the observed red giant sequence. This may be due to differences in metallicity or slight inaccuracies in the synthetic models. The observed stars redder than these early-M type stars – including the three M-type stars A, B and C – are not represented by the synthetic sequence. This may be due to the spectral-type dependence of the inter- and circumstellar reddening, which is especially important for intrinsically red objects towards the blue wavelengths. Large-amplitude pulsation of AGB stars may be responsible for weaker TiO absorption bands in the i-band (Schultheis et al. 1998). It may be noted that spectra are available for nearly all late-type AGB stars in the field, and that there are no strong candidates for carbon stars that have escaped notice other than the two identified.

Table 1. Optical, near- and mid-IR photometry for the six red stars in the HS 327 area. Coordinates have $\sim$1″ accuracy

Star	α (J2000.0)	δ (J2000.0)	g	r	i	K_s	[4.5]	[6.7]	[12]	[14.3]
Cluster members:										
IRAS 05298−6957	$5^h29^m24.5^s$	−69°55′14″	$\gtrsim$ 22.00	$\gtrsim$ 22.00	$\gtrsim$ 22.75	10.81	7.47	5.54	4.76	3.68
carbon	$5^h29^m25.1^s$	−69°54′53″	16.67	15.07	13.77	10.60	10.18	9.94	9.46	8.74
A	$5^h29^m24.2^s$	−69°55′42″	16.87	15.60	13.86	11.18	11.23	11.52	$\gtrsim$ 11.40	$\gtrsim$ 10.80
Field stars:										
red	$5^h29^m11.2^s$	−69°56′14″	20.07	17.23	15.89	11.15	9.18	8.75	8.55	8.60
B	$5^h29^m36.3^s$	−69°56′05″	17.36	15.83	13.93	11.20	11.10	10.80	10.77	11.18
C	$5^h29^m24.8^s$	−69°56′25″	16.70	15.12	12.93	9.75	9.74	9.60	9.60	9.71

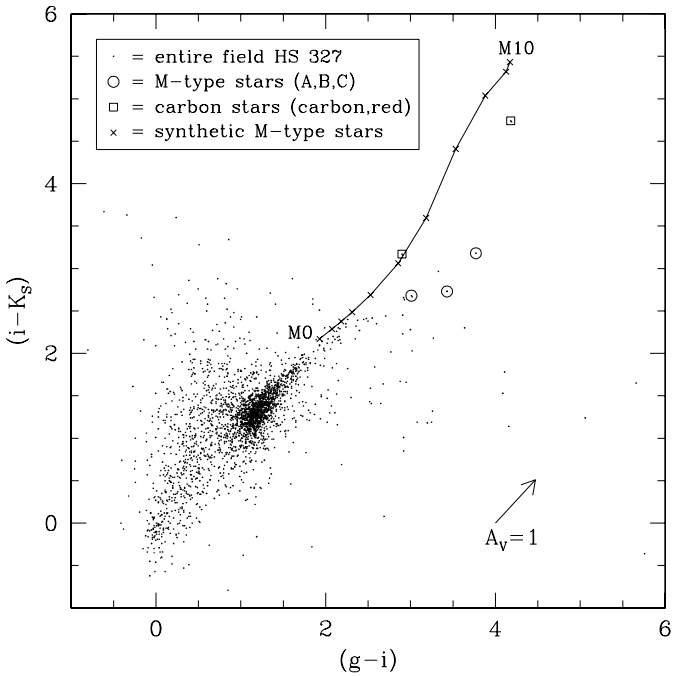

Fig. 7. $(i - K_s)$ versus $(g - i)$ colour-colour diagram for the stars in the field of HS 327. The M-type and carbon stars for which spectra have been obtained are indicated by circles and squares, respectively. Synthetic M-type spectra from Fluks et al. (1994) are plotted too (crosses, solid line)

3.7. Mid-IR photometry

Mid-IR images at wavelengths of 4.5, 6.7, 12 and 14.3 μ exist that cover the HS 327 area. These were obtained with the CAM instrument onboard ISO for the ISOGAL (Omont et al. 1999) and mini-survey (Loup et al. 1999) projects. The details of observation and data reduction as well as the catalogue with point source photometry will be described in a subsequent paper by Loup et al.

Only very few objects in the HS 327 area are bright enough in the mid-IR to have been detected by these ISO observations. Amongst these, IRAS 05298−6957, the carbon star, the "ABC" stars and the very red star are all detected in at least one of the mid-IR passbands, which can be used to better determine their bolometric luminosities. These stars also constitute six of the seven brightest stars in the K-band. Besides these stars that we had already identified as bright red giants on the basis of shorter wavelength data, no other such stars appear in the mid-IR images of the HS 327 area.

The mid-IR photometry is summarised in Table 1. Stars A and B and the carbon star are too faint and/or too close to IRAS 05298−6957 to have been included in the Loup et al. catalogue that was compiled using a homogeneous automatic multiple-object photometry procedure. Photometry is obtained by aperture photometry on the original images. The magnitudes follow the IRAS /ISO convention, with zero magnitudes of the LW1 (4.5 μm), LW2 (6.7 μm), LW10 (12 μm) and LW3 (14.3 μm) filters corresponding to 181.8, 89.5, 34.7 and 20.7 Jy, respectively. Additional near- and mid-IR photometry and spectroscopy for IRAS 05298−6957 can be found in Trams et al. (1999). This object was also detected by MSX (Price & Witteborn 1995) at 0.27 Jy in Band A (Egan et al. 1999), centred at 8.3 μm (range: 6.8 to 10.9 μm). Inspection of the MSX images (`http://www.ipac.caltech.edu/ipac/msx/msx.html`) reveals that IRAS 05298−6957 was also detected in Band D, centred at 14.6 μm, and that the red field carbon star was marginally detected at $\sim$0.03 Jy in Band A (below the nominal sensitivity limit). This is all consistent with the ISO photometry. The optical, near- and mid-IR photometry in Table 1 was gathered at different epochs, which is important because IRAS 05298−6957 – and possibly the other red stars as well – is a long-period variable star with a K-band amplitude of $\sim$2 mag (Wood et al. 1992). LW2 and LW10 observations are available for two epochs, for which the photometry was averaged.

The photometric SEDs of the six red stars near HS 327 are plotted in Fig. 8. IRAS 05298−6957 is optically invisible because of the severe circumstellar extinction by its massive dust envelope, whose emission produces a strong IR excess. The cluster carbon star does not suffer from much circumstellar extinction, but some IR excess emission is visible at the longest wavelengths. The field carbon star ("red") does experience significant extinction, but it is yet unclear whether it is of interstellar or of circumstellar origin. The three M giants are not noticeably reddened nor do they exhibit IR excess emission, and their mass-loss rates must therefore be very low: $\dot{M} \lesssim 10^{-8}\ M_\odot\ \mathrm{yr}^{-1}$ (see van Loon et al. 1999b). The derivation of accurate

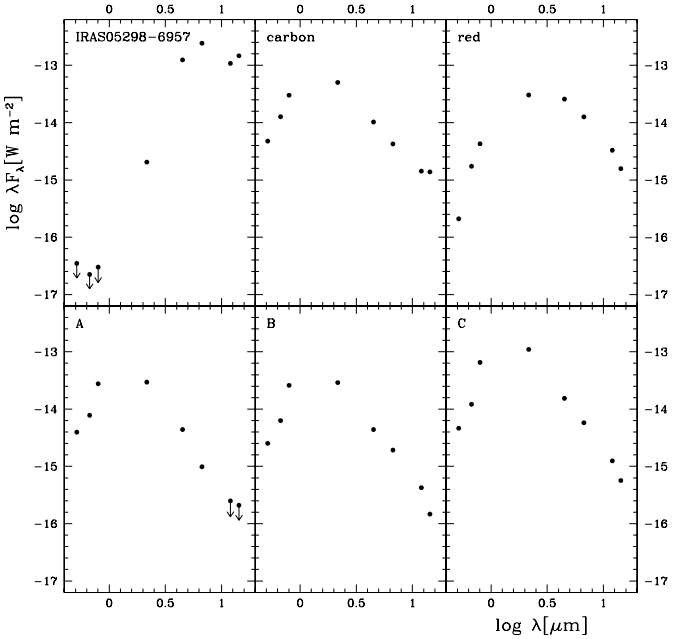

Fig. 8. SEDs of the red stars near HS 327

Table 2. Spectral types and luminosities

Star	Spectrum	$\log(L/L_\odot)$	$M_{\rm bol}$
Cluster members:			
IRAS 05298−6957	OH/IR	> 4.3	< -6.0
carbon	C4.5	3.8	−4.7
A	M 3	3.7	−4.5
Field stars:			
red	C	3.6	−4.3
B	M 5	3.7	−4.4
C	M 7	4.1	−5.6

mass-loss rates requires additional photometry at wavelengths of $\lambda \sim 20$ to 60 μm.

3.8. Luminosities

Bolometric luminosities (Table 2) are estimated by integrating under the SED. The luminosity derived for IRAS 05298−6957 here is consistent with the more complete derivation of the bolometric luminosity given by van Loon et al. (1999b): $M_{\rm bol} = -5.21$ to -6.72 mag. It is certainly the most luminous AGB star in the field. Both the cluster and field carbon stars are a few times less luminous, with luminosities typical for optically bright carbon stars (Costa & Frogel 1996). The red field star is less luminous than obscured carbon stars detected by IRAS (van Loon et al. 1997, 1998, 1999a,b).

3.9. Search for short-period variable stars

The imaging data comprises six nights of intensive observation, which would, in principle, allow the detection of variability on timescales of a few days and with amplitudes of the order of several tenths of a magnitude, e.g. Cepheids. To this aim we investigated the 46 individual r-band images, using only a single pass through DAOPHOT & ALLSTAR. The 4$^{\rm th}$ epoch (December 25) was taken as a reference, for it contained the largest number of extracted stars (4868). Of these, 3706 were recovered at least once more during the time series. The relative photometric calibration between the different epochs was improved by subtracting a baseline constructed from 146 stars that had been recovered at $\geq$30 epochs. All lightcurves were then checked by eye for variability. No convincing variable star candidates could be identified: a selection of $\sim$50 best cases were all consistent with variations due to inaccuracies in the source extraction and photometry.

Table 3. Relative number of the different classes of stars compared to their total, $n = N_i/N_{\rm tot}$, both for the cluster ($N_{\rm tot} = 480$) and the field ($N_{\rm tot} = 6739$) around HS 327. The cluster-over-field density, $\rho = N_{i,\rm cluster}/N_{i,\rm field}$, is corrected for the relative area (0.000334 and 0.003401 $\square^\circ$, respectively)

	Cluster	Field	ρ
MS_0	0.529 ± 0.041	0.541 ± 0.011	0.71 ± 0.05
MS_1	0.056 ± 0.011	0.049 ± 0.003	0.84 ± 0.17
MS_2	0.025 ± 0.007	0.014 ± 0.001	1.33 ± 0.41
Clump	0.125 ± 0.017	0.138 ± 0.005	0.66 ± 0.09
RGB	0.233 ± 0.024	0.247 ± 0.007	0.68 ± 0.07
AGB	0.031 ± 0.008	0.012 ± 0.001	1.86 ± 0.52

4. Discussion

4.1. The age of the HS 327 cluster

It is difficult to assess ages of the individual cluster stars. The locations in the CMD of the cluster carbon star and star "A" suggest ages of $t < 1$ Gyr for these stars, depending on the exact amount of interstellar reddening. For IRAS 05298−6957 an age cannot be derived directly from the CMD because of the difficulty to correct for its circumstellar extinction. It's luminosity of $\log(L/L_\odot) \gtrsim 4.3$ and likely evolutionary state at the very tip of its AGB suggests an age of $t \lesssim 500$ Myr (Bertelli et al. 1994).

The best indicators for the cluster age in the optical CMD are: (i) The compact red clump at $(g-i) = 1.1$, $i = 18.2$ and $(i-K_{\rm s}) = 1.2$, $K_{\rm s} = 16.8$ represents stars with ages $1 \lesssim t < 10$ Gyr; (ii) The bulk of the Main Sequence stars for which photometry could be extracted have ages of a few Gyr, but the data is incomplete for Main Sequence stars that are older; (iii) An extension of the Main Sequence to younger stars with ages $t \gtrsim 2\ 10^8$ yr; (iv) Luminous AGB stars with ages of a few $\times 10^8$ yr.

It is difficult to disentangle field and cluster due to the low contrast in stellar density (Figs. 1 and 6). In order to estimate whether the cluster belongs to the dominant field population of a few Gyr, or to the sparse younger field population of a few hundred Myr, statistics are obtained about the relative frequency of stars of different classes

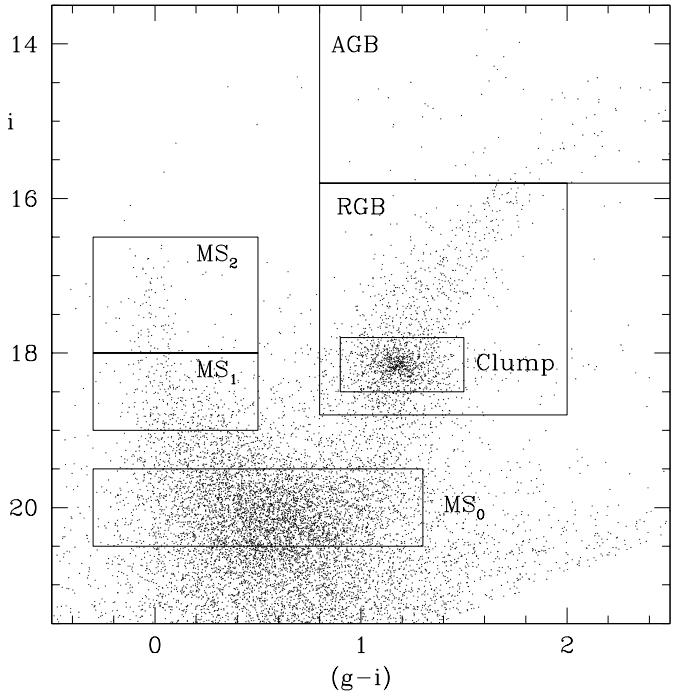

Fig. 9. HRD with all stars in and around HS 327, with indicated the areas for counting the different classes of stars

as defined in the CMD (Fig. 9): Main Sequence stars of a few Gyr (MS_0), $t \sim 500$ Myr to 1 Gyr (MS_1) and $t \sim 200$ to 500 Myr (MS_2); red clump stars, RGB stars of similar ages as the red clump stars, and AGB stars that generally represent ages of several hundred Myr. The counts are normalised to their sum (Table 3), and compared between cluster and field taking into account the differences in area.

Although the statistics are not striking, the different classes of stars all suggest that the cluster is associated with the younger population of a few hundred Myr (that is also present in the field), and that the older population of a few Gyr belongs entirely to the field. The statistics of the AGB stars and youngest Main Sequence stars in particular favours the interpretation of HS 327 having an age of $t \sim 200$ Myr. This agrees with the age of $t \sim 160 \pm 20$ Myr as derived by Pietrzyński & Udalski (2000a,b), which happens to correspond to an epoch of intensified star formation that also seems to have occurred in the field surrounding HS 327.

AGB stars seem to be relatively abundant within the cluster. As a simple consistency check, the number $N_{\rm MS}$ of Main-Sequence stars within a certain mass interval $[M_1, M_2]$ may be compared to the number $N_{\rm post}$ of post-Main Sequence stars within the mass interval $[M_3, M_4]$, where $M_2 = M_3 = 3.3\ M_\odot$ the current (200 Myr) Main-Sequence Turn-Off mass, and $M_4 = 4.0\ M_\odot$ the Main-Sequence progenitor mass corresponding to the current tip of the AGB (Bertelli et al. 1994). Assuming a Salpeter Initial Mass Function (Salpeter 1955)

$$\frac{{\rm d}N}{{\rm d}M} = \xi M^{-2.35} \qquad (1)$$

the observed $N_{\rm MS} = 12$ for $M_1 = 2.2\ M_\odot$ (500 Myr: MS_2) predicts $N_{\rm post} = 5$, and the observed $N_{\rm MS} = 81$ for $M_1 = 1.75\ M_\odot$ (1 Gyr: MS_1+MS_2) predicts $N_{\rm post} = 14$. These very rough estimates agree reasonably well with the observed $N_{\rm post} \sim 15$ ("AGB"). There are two TP-AGB stars (the carbon star and the OH/IR star) where less than one would be expected, but this is a bias as the cluster was studied exactly for reason of the presence of these two stars.

4.2. Cluster binarity

The LMC contains several populous binary clusters (Dieball et al. 2000; Dieball & Grebel 2000). HS 327 appears double (see also Pietrzyński & Udalski 2000a,b), showing that binarity also occurs amongst sparse open clusters. The moderate age of HS 327 implies that such clusters can resist tidal disruption for some while, although we do not know of course how many of HS 327's members have already been stripped off in the past.

There is some indication for a difference in the stellar content of the West and East components: HS 327-E is redder, or rather brighter in the $K_{\rm s}$ band. An analysis as performed in Table 3 but now comparing the East and West components of HS 327 suggests that HS 327-W might be somewhat younger than HS 327-E. Perhaps star formation in the West part was triggered by momentum input into the ISM by massive evolved stars in the East part. This result is not statistically significant, though, and Pietrzyński & Udalski (2000a,b) derive ages that are equal to within ∼50 Myr.

4.3. Progenitor masses of carbon stars and OH/IR stars

The obscured oxygen-rich AGB star IRAS 05298−6957 is more luminous than the cluster carbon star, which in its turn is more luminous than the oxygen-rich cluster star "A". Because these three stars have formed simultaneously, the sequence in luminosities strongly suggests a sequence in evolutionary state as a result of a sequence in progenitor mass, with IRAS 05298−6957 the most evolved and with the most massive progenitor. How can the sequence in chemistry be understood?

Intermediate-mass AGB stars become carbon stars as 3$^{\rm rd}$ dredge-up becomes effective on the upper AGB. This process is counteracted upon in massive AGB stars by carbon burning at the base of the convective mantle (HBB). Clearly, the progenitor mass of the cluster carbon star must be high enough to support 3$^{\rm rd}$ dredge-up but too low for the onset of HBB, whilst the progenitor of IRAS 05298−6957 was sufficiently massive for HBB to occur. Star "A" has yet to experience (enough) thermal pulses to become a carbon star.

The cluster age of $t \sim 200$ Myr implies a progenitor mass of $M_{\rm MS} \sim 4.0\ M_\odot$ for stars currently at the tip of the AGB (Bertelli et al. 1994). The range in progenitor

masses of stars along the AGB is less than 0.1 $M_\odot$. Hence the first direct measurement for the threshold mass above which HBB occurs indicates $M_{\rm HBB} \gtrsim 4.0\ M_\odot$.

This agrees well with current stellar evolution models. The lower and higher mass limits for carbon star formation in the LMC are currently believed to be $M_{\rm low} \sim 1.2$ and $M_{\rm high} \sim 4\ M_\odot$, respectively (Groenewegen & de Jong 1993; Marigo et al. 1999). Ventura et al. (1999) show that stars with $M_{\rm MS} \sim 3.8\ M_\odot$ first go through a short ($\Delta t \sim 30\,000$ yr) J-type (^{13}C-enhanced) carbon star phase before HBB converts them back into oxygen-rich stars. Because of the short lifetime and the lack of evidence for ^{13}C enhancement, it is unlikely that the cluster carbon star is currently going through this peculiar evolutionary phase. It is possible that IRAS 05298−6957 may have done so in the past, though.

However, as the referee rightfully pointed out, it is difficult to reconcile the low luminosity of the cluster carbon star with a 4 $M_\odot$ TP-AGB star. Stellar evolution models (Marigo et al. 1999) predict that for a star with $M_{\rm MS} \sim 4.0\ M_\odot$ the onset of the TP-AGB occurs around $M_{\rm bol} \sim -6$ mag. The luminosity of the cluster carbon star of $M_{\rm bol} \sim -4.7$ mag would rather suggest $M_{\rm MS} \lesssim 3.0\ M_\odot$. The star may have been fainter than average due to either stellar surface pulsations, a post-TP luminosity dip or both, but it is unlikely that this would account for a difference of ∼1.3 mag. It is also possible, but unlikely, that the carbon star is not a cluster member. We therefore suggest that current stellar models over-estimate the core mass (i.e. luminosity) at which AGB stars with $M_{\rm MS} \sim 4.0\ M_\odot$ start to experience 3$^{\rm rd}$ dredge-up.

Acknowledgements. We are grateful for generous allocation by ESO of Director's Discretionary Time. This work has benefitted from the use of the SIMBAD database, operated at CDS, Strasbourg, France, and the Second Generation Digitized Sky Survey, produced at the Space Telescope Science Institute under U.S. Government grant NAG W-2166 and based on photographic data obtained using the Oschin Schmidt Telescope on Palomar Mountain and the UK Schmidt Telescope. We thank Fernando Comerón for help with the SOFI observations and for reading an earlier version of the manuscript. We also thank the referee for her/his valuable suggestions. O Jacco se sente muito afortunado ser gémeos unidos com o anjinho Joana.

Appendix A: Photometric standard stars

The standard stars used for the photometry in the Gunn system are listed in Table A.1, together with their magnitudes from the literature (Thuan & Gunn 1976; Wade et al. 1979) and from our observations during the five nights from December 25 to 29, 1996. Of these, HD 19445 and BD+21 607 are used as primary standards because these are the only stars in our set that have known i-band magnitudes. Ross 683 and especially Ross 889 showed the largest discrepancies with respect to the full set of standard stars, and their use as standard stars may therefore be questioned. Ross 374 and Ross 786 were found to be in good agreement with their literature magnitudes. The magnitudes determined here are accurate to ∼0.01 mag.

Table A.1. Photometric standard stars for the Gunn system

Star	literature			observed		
	g	r	i	g	r	i
BD+21 607	9.25	9.26	9.27	9.25	9.26	9.27
HD 19445	8.088	8.070	8.070	8.09	8.07	8.07
Ross 374	10.851	10.772		10.85	10.77	10.74
Ross 683	11.40	11.08		11.38	11.12	11.04
Ross 786	10.06	9.81		10.03	9.81	9.73
Ross 889	10.43	10.51		10.20	10.27	10.35

References

Aaronson, M., & Mould, J. 1985, ApJ, 288, 551
Barnbaum, C., Stone, R. P. S., & Keenan, P. C. 1996, ApJS, 105, 419
Bertelli, G., Bressan, A., Chiosi, C., Fagotto, F., & Nasi, E. 1994, A&AS, 106, 275
Boothroyd, A. I., Sackmann, I.-J., & Ahern, S. C. 1993, ApJ, 416, 762
Costa, E., & Frogel, J. A. 1996, AJ, 112, 2607
Dieball, A., & Grebel, E. K. 2000, A&A, 358, 897
Dieball, A., Grebel, E. K., & Theis, C. 2000, A&A, 358, 144
Egan, M. P., et al. 1999, in Astrophysics with Infrared Surveys, A Prelude to SIRTF, ed. M. D. Bicay, R. M. Cutri, & B. F. Madore, ASP Conf. Ser., 177, 404
Fluks, M. A., Plez, B., Thé, P. S., et al. 1994, A&AS, 105, 311
Frost, C. A., Cannon, R. C., Lattanzio, J. C., Wood, P. R., & Forestini, M. 1998, A&A, 332, L17
Groenewegen, M. A. T., & de Jong, T. 1993, A&A, 267, 410
Hodge, P. W., & Sexton, J. A. 1966, AJ, 71, 363
Iben, I. 1981, ApJ, 246, 278
Iben, I., Renzini, A. 1983, ARA&A, 21, 271
Kontizas, E., Metaxa, M., & Kontizas, M. 1988, AJ, 96, 1625
Kurucz, R. L. 1993, Kurucz CD-ROM, Smithsonian Astrophysical Observatory, Cambridge MA
Loup, C., Cioni, M. R., & Blommaert, J. A. D. L. 1999, in The Universe as Seen by ISO, ed. P. Cox, & M. F. Kessler, ESA-SP 427, 369
Marigo, P., Bressan, A., & Chiosi, C. 1998, A&A, 331, 564
Marigo, P., Girardi, L., & Bressan, A. 1999, A&A, 344, 123
Mathis, J. S., ARA&A, 28, 37
Omont, A., 1999, The ISOGAL Collaboration, in The Universe as Seen by ISO, ed. P. Cox, & M. F. Kessler, ESA-SP, 427, 211
Pietrzyński, G., & Udalski, A. 2000a, Acta Astron., 50, 337
Pietrzyński, G., & Udalski, A. 2000b, Acta Astron., 50, 355
Price, S. D., & Witteborn, F. C. 1995, in Airborne Astronomy Symposium on the Galactic Ecosystem: From Gas to Stars to Dust, ed. M. R. Haas, J. A. Davidson, & E. F. Erickson, ASP Conf. Ser., 73, 685
Salpeter, E. E. 1955, ApJ, 121, 161
Schultheis, M., Aringer, B., Höfner, S., & Jorgensen, U. 1998, in Asymptotic Giant Branch Stars, ed. T. Le Bertre, A. Lèbre, & C. Waelkens, ASP Conf. Ser., 614
Stetson, P. B. 1987, PASP, 99, 191
Tanabé, T., Nishida, S., Matsumoto, S., et al. 1997, Nature, 385, 509
Thuan, T. X., & Gunn, J. E. 1976, PASP, 88, 543

Trams, N. R., van Loon, J. Th., Waters, L. B. F. M., et al. 1999a, A&A, 344, L17
Trams, N. R., van Loon, J. Th., Waters, L. B. F. M., et al. 1999b, A&A, 346, 843
Turnshek, D. E., Turnshek, D. A., Craine, E. R., & Boeshaar, P. C. 1985, An atlas of digital spectra of cool stars (Western Research Company, Tucson)
van Loon, J. Th., Zijlstra, A. A., Whitelock, P. A., et al. 1997, A&A, 325, 585
van Loon, J. Th., Zijlstra, A. A., Whitelock, P. A., et al. 1998, A&A, 329, 169
van Loon, J. Th., Zijlstra, A. A., & Groenewegen, M. A. T. 1999a, A&A, 346, 805
van Loon, J. Th., Groenewegen, M. A. T., de Koter, A., et al. 1999b, A&A, 351, 559
Ventura, P., D'Antona, F., & Mazzitelli, I. 1999, ApJ, 524, L111
Wade, R. A., Hoessel, J. G., Elias, J. H., & Huchra, J. P. 1979, PASP, 91, 35
Westerlund, B. E., Azzopardi, M., Breysacher, J., & Rebeirot, E. 1991, A&AS, 91, 425
Wood, P. R., Bessell, M. S., & Fox, M. W. 1983, ApJ, 272, 99
Wood, P. R., Whiteoak, J. B., Hughes, S. M. G., et al. 1992, ApJ, 397, 552